Methods

Histopathological examination

Autopsied brain was fixed in 10% buffered formalin and processed into paraffin sections. Sections were routinely stained with hematoxylin and eosin (H&E) and by Klüver–Barrera (KB) staining and Bodian staining. The antibodies used in this study included anti-phosphorylated neurofilament (DakoCytomation, Denmark, mouse monoclonal, clone 2F11) used at 1:200, anti-glial fibrillary acidic protein (GFAP) (DakoCytomation, rabbit polyclonal) used at 1:1,000, and anti-CD68 (DakoCytomation, mouse monoclonal, clone KP1) used at 1:200. All sections were deparaffinized and endogenous peroxidase activity was blocked with 0.3% H_2O_2/methanol. After overnight incubation with primary antibody at 4°C, sections were subjected to the streptavidin biotin complex method. Immunoreactivity was detected using 3,3′-diaminobenzidine (DAB), and sections were counterstained with hematoxylin.

Sequence analysis of the PLP1 gene

Genomic DNA was isolated from the frozen autopsied brain of the patient using ISOGEN (Nippon Gene, Japan). All seven exons of *PLP1* were amplified by PCR using intronic primers [15]. The PCR product was sequenced using a BigDye Terminator Sequencing Kit (Applied Biosystems, Carlsbad, CA, USA). Sequencing reactions were loaded on an automated Applied Biosystems Model 3100 DNA sequencer. This study was approved by the Ethics Committee of Kyushu University, Faculty of Medicine.

Case presentation

The patient was a 67-year-old man.

Family history. No consanguineous marriage. The patient was the youngest of six siblings. A brother immediately senior to the patient developed gait disturbance due to stiffness of the lower limbs associated with dementia in his 40 s, and died of the disease.

Past history. Not eventful.

Life history. No smoking. One cup of sake/day for 10 years until 14 years after onset.

Clinical history. The patient developed a flat-footed gait 33 years before death at the age of 35. The gait difficulty gradually progressed, and limping of the left lower limb became apparent by 6 years after onset. Gait disturbance rapidly progressed, and the patient became wheelchair-bound by 10 years after onset. Fourteen years after onset, he developed urinary incontinence, and lost independence in daily life. A bladder catheter was placed, and the patient was hospitalized thereafter. At this point, he was able to rise, wheelchair-mobile, but unable to walk. He gradually developed dementia, and scored 7.5/30 (cut off being 20 points) on the Revised Hasegawa's Dementia Scale test 16 years after onset. By 28 years after onset, he became tube-fed due to dysphagia. By this time, he also became speechless and bed-ridden. He repeatedly developed pneumonia, ileus, liver dysfunction, troubles with the bladder catheter due to urolithiasis, and bronchial asthma. His neurological status had been stable, and at 29 years after onset, he was capable of eye-opening upon verbal command and pursuit eye movement. He developed pneumonia 4 days before death, and died of respiratory failure. Autopsy was performed 15 h after death. Appropriate informed consent was obtained from the family.

Radiographical findings. Computed tomography (CT) images were available during the period from 14 to 23 years after onset (Fig. 1). Diffuse low density of the white matter was already evident at 14 years after onset, suggesting leukoencephalopathy. Thinning of the corpus callosum was also appreciated at this point. During the following 9 years, progressive enlargement of the cortical sulci and dilatation of the ventricular system were observed.

Pathological findings. At autopsy, moderate atrophy and contracture of the skeletal muscles of the bilateral upper and lower extremities were noted. Brain weight was 1,275 g. Although a diffuse, mild atrophy of the cerebral cortex was seen, the gross external appearance of the brain was within the normal limit. Coronal sectioning of the cerebrum revealed focal discoloration and softening of the white matter, which was especially highlighted in the parieto-occipital lobes associated with diffuse, moderate dilatation of the ventricular system (Fig. 2a). Severe thinning of the corpus callosum was also noted (Fig. 2a, b). Histopathologically, KB staining revealed widespread myelin loss throughout the central nervous system (CNS) including the optic nerves (Figs. 2b–e, 3, 4a, 5b) while the cerebral cortex was well preserved with only mild gliosis (data not shown). Silver impregnation and immunohistochemistry for neurofilament showed relative preservation of the axonal fibers, although various degrees of axonal loss or degeneration were noted (Figs. 4d, 5e–g, i, see below for details). These findings indicated that the myelin was primarily affected in the white matter lesions, indicating a demyelinating disease. The spinal cord and medulla oblongata exhibited diffuse, severe myelin loss in the white matter tracts. However, the myelin of the peripheral nervous system (PNS) was well preserved (Figs. 3d, 4a–c). The pons, cerebellum, and midbrain also showed diffuse myelin loss (Fig. 3); however, there were some specific white matter tracts that were more severely

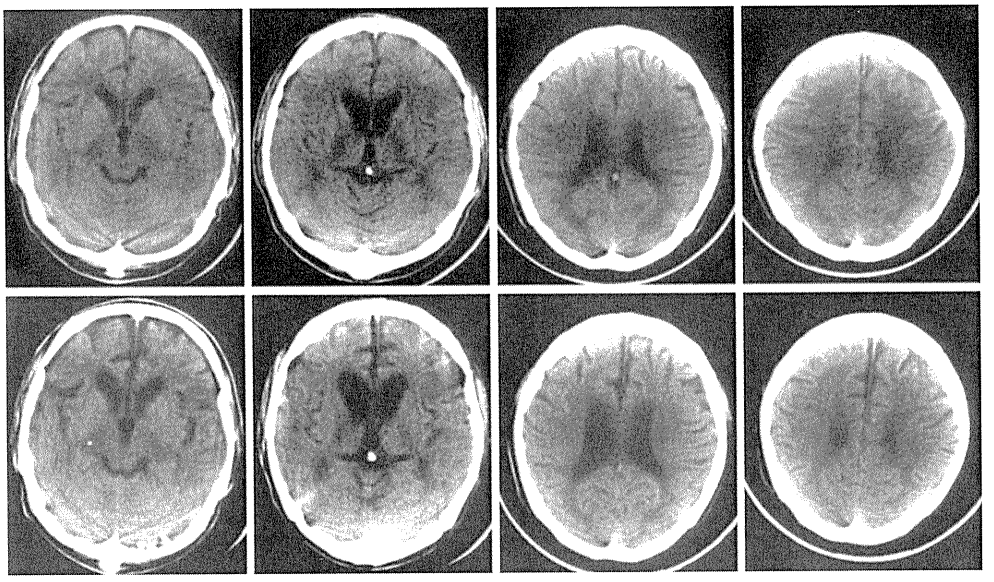

Fig. 1 CT scan showing long-term, progressive degeneration of the white matter accompanied by dilatation of the ventricular system. Thinning of the corpus callosum can be seen. *Upper panel* 14 years after onset, *lower panel* 23 years after onset

affected. These included the pyramidal tracts, the tracts in the pontine tegmentum including the superior cerebellar peduncles, central tegmental tracts, medial longitudinal tracts and the medial lemniscus (Fig. 3).

In addition to myelin loss, immunostaining for phosphorylated neurofilament in these severely affected white matter tracts revealed prominent axonal loss accompanied by swelling of the remaining fibers and spheroid formation (Figs. 4d, 5e–g, i). In the affected white matter, only mild to moderate gliosis was revealed by GFAP immunostaining (Fig. 5c). Immunohistochemistry for CD68 revealed scattering infiltration of foamy macrophages (Fig. 5d) and perivascular accumulation of lymphocytes was not evident. In the cerebellum, mild loss of the granule cells and moderate loss of Purkinje cells with torpedo formation were noted (Fig. 5g). The white matter of the cerebellum also showed both myelin (Fig. 3a) and axonal loss (Fig. 5g). We observed grumose degeneration of the dentate nucleus (Fig. 5h) and severe myelin and axonal loss in the hilus of the dentate nucleus through to the superior cerebellar peduncle (Figs. 3a, c, 5i).

Sequence analysis of the PLP1 gene

Direct sequencing revealed an A>G transition in exon 7 of *PLP1* that results in a tyrosine to cysteine substitution at residue 263 of the PLP1 protein (c.788A>G (p.Tyr263-Cys)). This amino acid residue, located in the fourth transmembrane domain (TM4) of PLP1, is highly conserved across species. This mutation was absent in 150 unrelated normal alleles.

Discussion

Hereditary spastic paraplegia is a genetically heterogeneous group of disorders characterized by progressive lower-extremity spasticity and weakness [2]. The current case presented with late–onset progressive spastic gait with other neurologic abnormalities such as bladder incontinence and dementia. Family history indicated X-linked or autosomal recessive inheritance. Pathological examination revealed widespread myelin loss in the white matter of the CNS, but not in the PNS. We therefore examined the sequence of *PLP1*, a causative gene for X-linked SPG2 and found a novel mutation, p.Tyr263Cys. Of note, the ages of onset of SPG2 patients reported to date range from 1 to 18 years [18, 22]. As far as we know, this is the first report of an SPG2 patient with a *PLP1* mutation and onset after the third decade of life.

PLP1 is the most abundant component of CNS myelin and is mainly expressed in oligodendrocytes [13]. Different *PLP1* abnormalities, including entire gene duplication, deletion, translocation and point mutations, result in a broad spectrum of *PLP1*-related disorders. Different missense mutations in particular lead to a variety of phenotypes from the most severe dysmyelinating form (connatal PMD) to mild forms of SPG2 [1, 3, 14, 20, 25]. The distinction between PMD and SPG2 is mainly based on clinical manifestations. PMD typically manifests in infancy or early childhood with nystagmus, hypotonia and cognitive impairment, which progress to severe spasticity and ataxia, and life span is shortened. In comparison, SPG2 manifests as spastic paraparesis with (complicated form) or

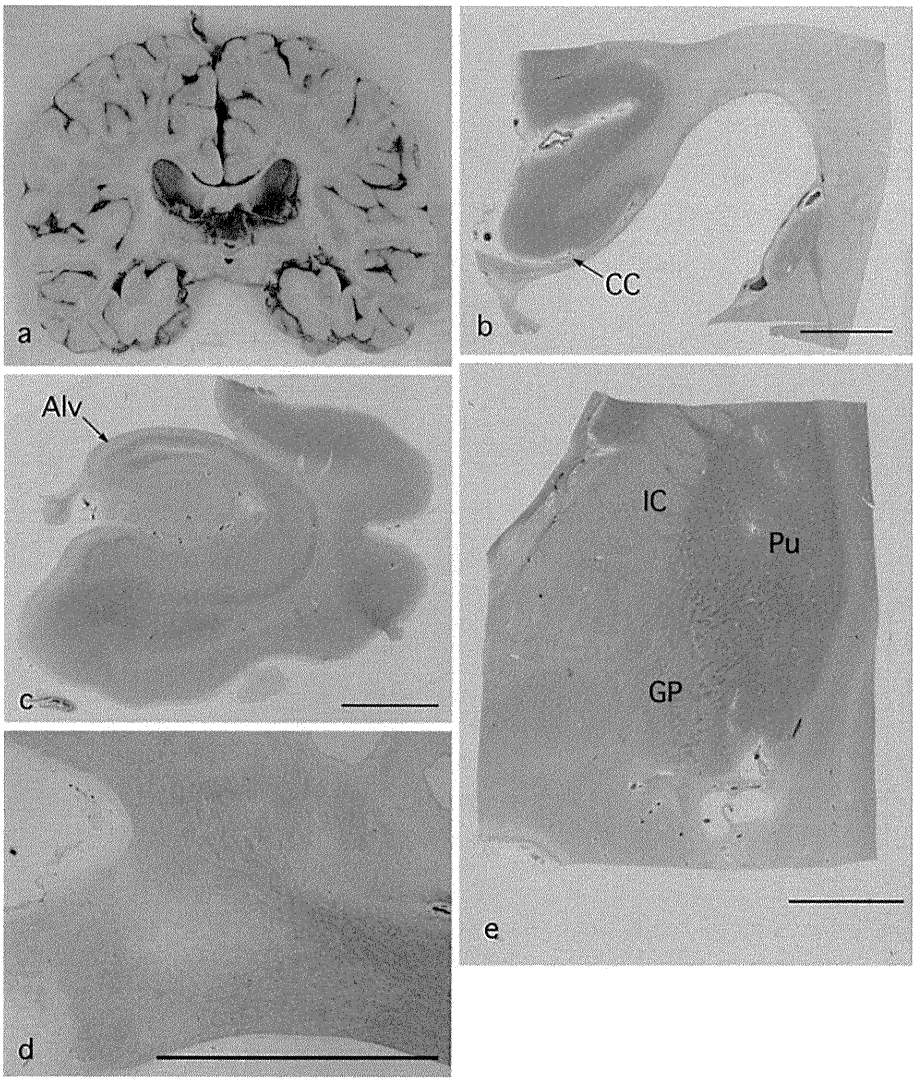

Fig. 2 Pathological changes in the cerebrum. **a** Macroscopic appearance of the cerebrum, **b–e** Klüver–Barrera staining. **a** Coronal section of the cerebrum at the level of the pulvinar. The dilatation of the ventricular system and discoloration of the white matter especially in the dorsal portion. The cerebral cortex is grossly preserved. **b** Coronal section at the level of the anterior cingulate gyrus. Diffuse myelin pallor is evident. The corpus callosum shows severe thinning. **c** Hippocampus. The white matter including the alveus hippocampi shows severe demyelination. **d** Optic chiasma. Patchy demyelination can be seen. **e** Basal ganglia. The internal capsule shows demyelination. *CC* corpus callosum, *Alv* alveus hippocampi, *IC* internal capsule, *Pu* putamen, *GP* globus pallidus. *Bar* 5 mm

without (uncomplicated form) CNS involvement and may develop later in life. Patients usually have a normal life span. Our case meets the criteria for the complicated form of SPG2 [1–3, 14, 20, 25].

Mutations that affect the folding and transport to the cell surface of PLP1 are associated with connatal PMD and also increased oligodendrocyte cell death [5–7, 23, 24]. Mutations in exon 3B of *PLP1* might predominantly result in SPG2 rather than PMD because this exon is spliced out in DM20, which therefore is supposed to be left intact [1, 10, 19, 20, 22]. Several mutations in exons 4, 5 and 6 have also been reported in SPG2 patients [9, 16, 18]. However, in general, there is no clear one-to-one correlation between the clinical courses and locations of the mutations [1, 11].

We have previously reported a single base insertion (c.774_775insG) at exon 7 that may lead to a frame-shift event, production of a truncated PLP1 protein (p.Ile259AspfsX11), and a classical type PMD [17]. However, this is the first report of a missense mutation in exon 7 of *PLP1*. The following evidence supports a causative role for the Tyr263Cys mutation in the pathogenesis of SPG2. This mutation was absent in 150 normal alleles. The amino acid at residue 263 is well conserved across PLP1 homologs of various vertebrate species. PLP1 is a highly conserved protein and 100% identical between humans and mice [12].

This last exon encodes the C-terminal 23 amino acids (residues 255–277), part of the fourth transmembrane domain and intracellular residues [3]. The mutation we found is located in the transmembrane domain. Considering this finding together with the late–onset, long-term clinical course of the present case, this mutation may have a subtle effect on the PLP1 structure, which may not cause oligodendrocyte death during early brain development, but which may influence the maintenance of the myelin structure and functions. Further analysis is necessary to clarify the pathogenesis of SPG2 and the function of PLP1 in the maintenance of myelin.

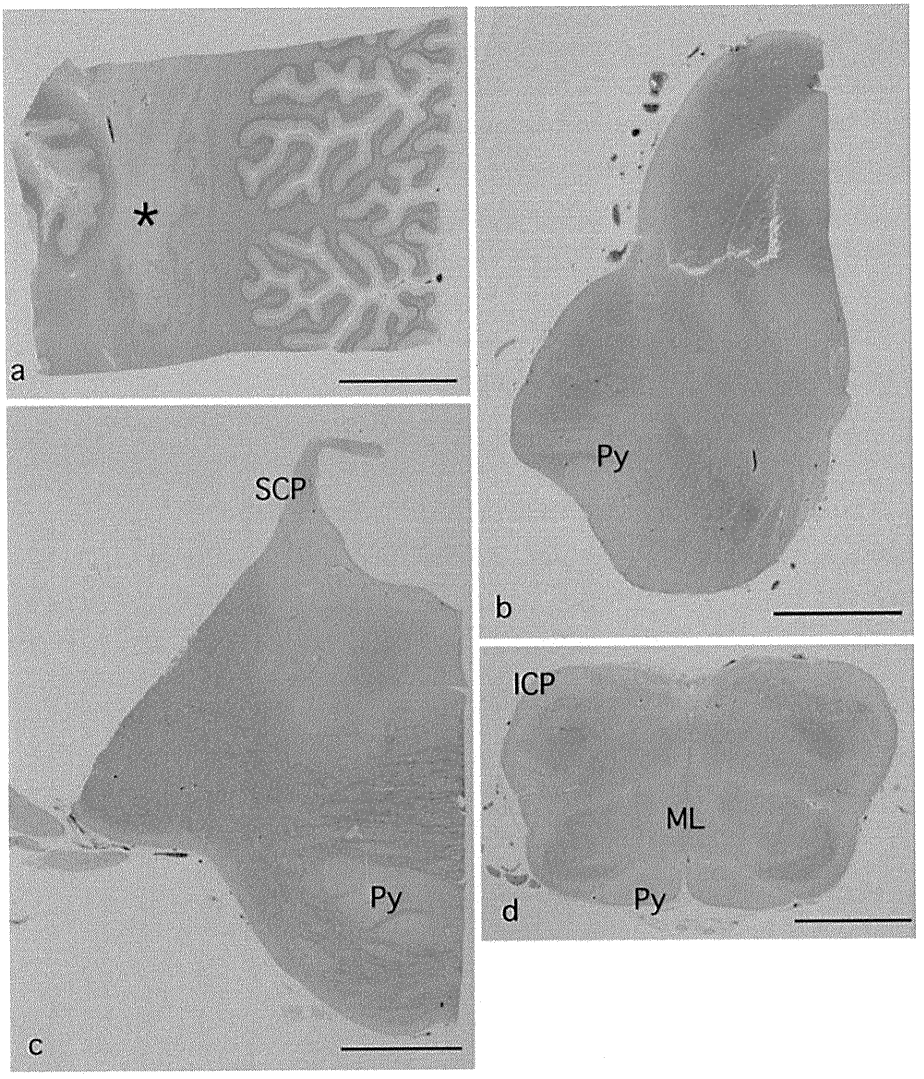

Fig. 3 Pathological changes in the cerebellum and the brainstem. **a–d** Klüver–Barrera staining. **a** Cerebellum, **b** midbrain, **c** pons, **d** medulla oblongata. Prominent myelin loss can be seen in some selected white matter tracts including the hilus of the dentate nucleus (*asterisk*, **a**) continuing to the superior cerebellar peduncle (*SCP*, **c**), the pyramidal tract (*Py*, **b–d**), medial lemniscus (*ML*, **d**) and the inferior cerebellar peduncle (*ICP*, **d**). *Bar* 5 mm

The neuropathological findings in the current case reflect the long-term clinical course of SPG2: widespread myelin loss throughout the CNS with relatively preserved axons except for some select white matter tracts, preservation of peripheral nerve myelin, mild gliosis and inflammatory infiltration including that of macrophages. The so-called tigroid pattern, i.e. patchy demyelinating lesions typical of early-onset PMD, was not noted except at the optic chiasm.

Of note, although widespread demyelination was observed, distinct white matter tracts were predominantly affected. These included the corpus callosum, the corticospinal tract, the medial lemniscus, and the superior cerebellar peduncle. We observed severe axonal degeneration in these white matter tracts. Axonal degeneration and/or neuronal loss have been reported both in rodent models [4, 8] and human subjects [8, 21] with *PLP1* deficiency. Although the precise mechanism underlying neuronal degeneration in cases of *PLP1* deficiency is not fully understood, these authors speculate that disruption of PLP1-mediated axonal–glial interactions may cause secondary axonal degeneration [4, 8, 21]. Despite the prominent degeneration of myelinated fibers, the number of neuronal somata in the cerebral cortex was well preserved in the present case. Similarly, while severe loss of cerebellar white matter axons, grumose degeneration of the dentate neurons and axonal degeneration in the hilus of the dentate nucleus were noted, the loss of Purkinje cells and dentate neurons was only mild. Because this case had a slowly progressive disease course, we posit that axonal degeneration did not cause neuronal loss by the time of the patient's death.

Gerbern et al. observed length-dependent axonal degeneration in *plp*-null animals and patients [24]. It is tempting to speculate that the *PLP1* mutation in the present case causes debilitation of once-formed myelin and axons over a period of decades, in not only a length-dependent but also an activity-dependent manner, because these long

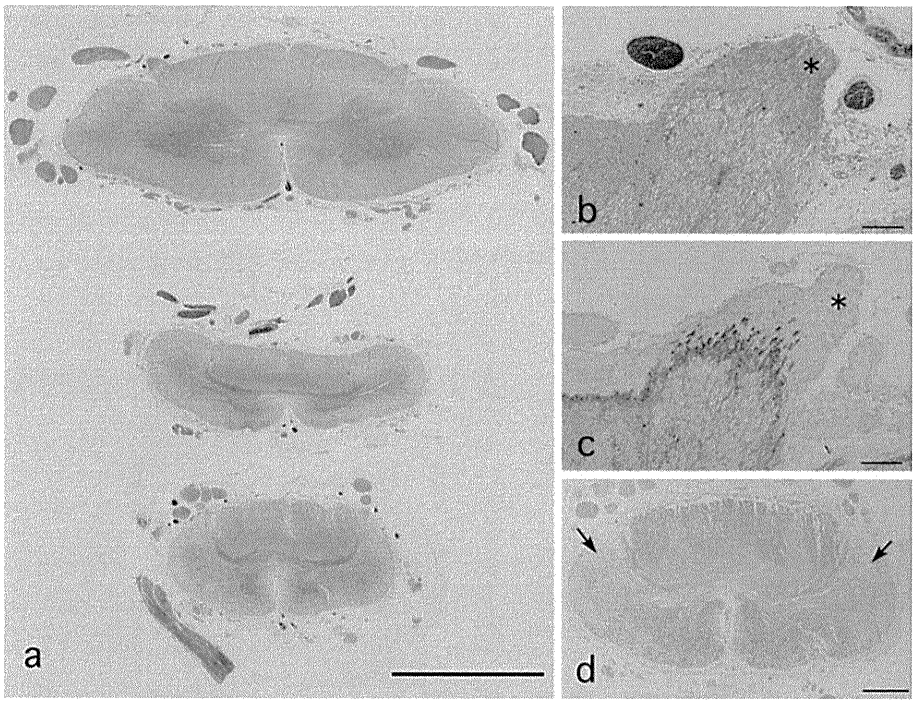

Fig. 4 Pathological changes in the spinal cord. **a**, **b** Klüver–Barrera staining, **c** GFAP immunostaining, **d** phosphorylated neurofilament staining. **a** The diffuse, severe CNS demyelination throughout the spinal cord in contrast to the preserved PNS myelin of the spinal nerve roots. **b**, **c** The entry zone of the dorsal root shows a jagged edge of the gliotic CNS portion contrasted by preserved myelination in the PNS portion (*asterisks*). **d** Neurofilament immunostaining showing diffuse axonal loss, which is most prominent in the corticospinal tract. *Bar* 5 mm (**a**), 200 μm (**b**, **c**), 1 mm (**d**)

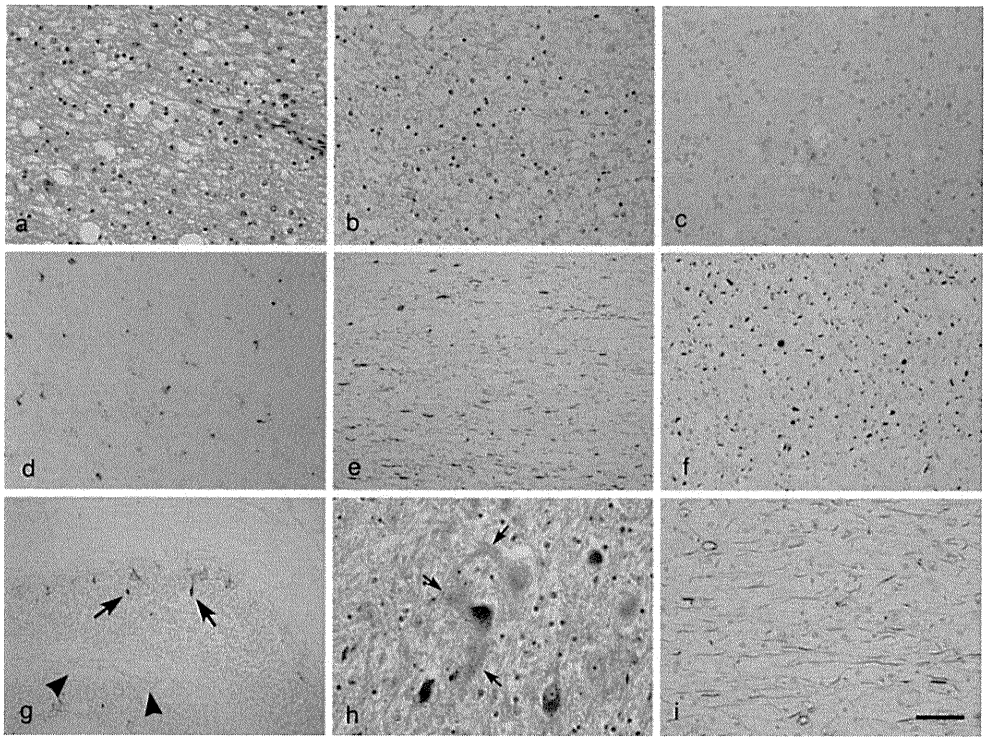

Fig. 5 Microscopic features of the brain. **a** H&E staining, **b**, **h** Klüver–Barrera staining, **c** GFAP immunostaining, **d** CD68 immunostaining, **e**–**g**, **i** phosphorylated neurofilament immunostaining. **a**–**d** The white matter of the frontal lobe. Although the white matter shows severe demyelination and mild vacuolation (**a**, **b**), perivascular lymphocytic cuffing is absent (**a**), and gliosis (**c**) and infiltration of the macrophages (**d**) are very mild. **e**, **f** Corpus callosum (**e**) and medullary pyramid (**f**). In addition to severe demyelination, axonal loss accompanied by spheroid formation is noted in these white matter tracts. **g**–**i** Cerebellum. Occasional torpedoes (*arrows*) and prominent axonal loss (*arrowheads*) are noted (**g**). The dentate nucleus shows grumose degeneration (*arrows*) (**h**). The hilus of the dentate nucleus also shows severe axonal loss (**i**). *Bar* 100 μm (**a**–**d**, **f**, **i**), 200 μm (**e**), 400 μm (**g**), 40 μm (**h**)

tracts and cerebellar input–output systems are thought to represent highly active conduction pathways.

Further analysis is necessary to clarify the pathogenesis of SPG2 and the function of PLP1 in the maintenance of myelin.

Acknowledgments This work was supported in part by a Health and Labour Sciences Research Grant from the Ministry of Health, Labour and Welfare of Japan (A.I.). The authors thank Ms. Sachiko Koyama (Dept. of Neuropathology, Kyushu University) for her excellent technical support.

References

1. Cailloux F, Gauthier-Barichard F, Mimault C et al (2000) Genotype-phenotype correlation in inherited brain myelination defects due to proteolipid protein gene mutations. Clinical European network on brain dysmyelinating disease. Eur J Hum Genet 8:837–845
2. Fink JK, Heiman-Patterson T, Bird T et al (1996) Hereditary spastic paraplegia: advances in genetic research. Hereditary Spastic Paraplegia Working group. Neurology 46:1507–1514
3. Garbern JY (2007) Pelizaeus-Merzbacher disease: genetic and cellular pathogenesis. Cell Mol Life Sci 64:50–65
4. Garbern JY, Yool DA, Moore GJ et al (2002) Patients lacking the major CNS myelin protein, proteolipid protein 1, develop length-dependent axonal degeneration in the absence of demyelination and inflammation. Brain 125:551–561
5. Gow A, Friedrich VL Jr, Lazzarini RA (1994) Many naturally occurring mutations of myelin proteolipid protein impair its intracellular transport. J Neurosci Res 37:574–583
6. Gow A, Lazzarini RA (1996) A cellular mechanism governing the severity of Pelizaeus–Merzbacher disease. Nat Genet 13:422–428
7. Gow A, Sharma R (2003) The unfolded protein response in protein aggregating diseases. Neuromol Med 4:73–94
8. Griffiths I, Klugmann M, Anderson T et al (1998) Axonal swellings and degeneration in mice lacking the major proteolipid of myelin. Science 280:1610–1613
9. Grossi S, Regis S, Biancheri R et al (2011) Molecular genetic analysis of the PLP1 Gene in 38 families with PLP1-related disorders: identification and functional characterization of 11 Novel PLP1 mutations. Orphanet J Rare Dis 6:40
10. Hodes ME, Blank CA, Pratt VM, Morales J, Napier J, Dlouhy SR (1997) Nonsense mutation in exon 3 of the proteolipid protein gene (PLP) in a family with an unusual form of Pelizaeus–Merzbacher disease. Am J Med Genet 69:121–125
11. Hodes ME, Zimmerman AW, Aydanian A et al (1999) Different mutations in the same codon of the proteolipid protein gene, PLP, may help in correlating genotype with phenotype in Pelizaeus–Merzbacher disease/X-linked spastic paraplegia (PMD/SPG2). Am J Med Genet 82:132–139
12. Hudson LD, Berndt JA, Puckett C, Kozak CA, Lazzarini RA (1987) Aberrant splicing of proteolipid protein mRNA in the dysmyelinating jimpy mutant mouse. Proc Natl Acad Sci USA 84:1454–1458
13. Hudson LD, Friedrich VL Jr, Behar T, Dubois-Dalcq M, Lazzarini RA (1989) The initial events in myelin synthesis: orientation of proteolipid protein in the plasma membrane of cultured oligodendrocytes. J Cell Biol 109:717–727
14. Inoue K (2005) PLP1-related inherited dysmyelinating disorders: Pelizaeus–Merzbacher disease and spastic paraplegia type 2. Neurogenetics 6:1–16
15. Iwaki A, Muramoto T, Iwaki I et al (1993) A missense mutation in the proteolipid protein gene responsible for Pelizaeus–Merzbacher disease in a Japanese family. Hum Mol Genet 2:19–22
16. Kobayashi H, Hoffman EP, Marks HG (1994) The rumpshaker mutation in spastic paraplegia. Nat Genet 7:351–352
17. Kurosawa K, Iwaki A, Miyake S, Imaizumi K, Kuroki Y, Fukumaki Y (1993) A novel insertional mutation at exon VII of the myelin proteolipid protein gene in Pelizaeus–Merzbacher disease. Hum Mol Genet 2:2187–2189
18. Lee ES, Moon HK, Park YH, Garbern J, Hobson GM (2004) A case of complicated spastic paraplegia 2 due to a point mutation in the proteolipid protein 1 gene. J Neurol Sci 224:83–87
19. Osaka H, Koizume S, Aoyama H et al (2010) Mild phenotype in Pelizaeus–Merzbacher disease caused by a PLP1-specific mutation. Brain Dev 32:703–707
20. Saugier-Veber P, Munnich A, Bonneau D et al (1994) X-linked spastic paraplegia and Pelizaeus–Merzbacher disease are allelic disorders at the proteolipid protein locus. Nat Genet 6:257–262
21. Sima AA, Pierson CR, Woltjer RL et al (2009) Neuronal loss in Pelizaeus–Merzbacher disease differs in various mutations of the proteolipid protein 1. Acta Neuropathol 118:531–539
22. Sivakumar K, Sambuughin N, Selenge B et al (1999) Novel exon 3B proteolipid protein gene mutation causing late-onset spastic paraplegia type 2 with variable penetrance in female family members. Ann Neurol 45:680–683
23. Southwood CM, Garbern J, Jiang W, Gow A (2002) The unfolded protein response modulates disease severity in Pelizaeus–Merzbacher disease. Neuron 36:585–596
24. Thomson CE, Montague P, Jung M, Nave KA, Griffiths IR (1997) Phenotypic severity of murine Plp mutants reflects in vivo and in vitro variations in transport of PLP isoproteins. Glia 20:322–332
25. Woodward KJ (2008) The molecular and cellular defects underlying Pelizaeus–Merzbacher disease. Expert Rev Mol Med 10:e14

ARTICLE IN PRESS

YMGME-05243; No. of pages: 7; 4C: 3, 4

Molecular Genetics and Metabolism xxx (2012) xxx–xxx

Contents lists available at SciVerse ScienceDirect

Molecular Genetics and Metabolism

journal homepage: www.elsevier.com/locate/ymgme

Effect of curcumin in a mouse model of Pelizaeus–Merzbacher disease

Li-Hua Yu [a], Toshifumi Morimura [a], Yurika Numata [a], Ryoko Yamamoto [a], Naoko Inoue [a], Barbara Antalfy [b], Yu-ichi Goto [a], Kimiko Deguchi [a,c], Hitoshi Osaka [d], Ken Inoue [a,*]

[a] Department of Mental Retardation and Birth Defect Research, National Institute of Neuroscience, National Center of Neurology and Psychiatry, Kodaira, Japan
[b] Department of Pathology, Texas Children's Hospital, Houston, USA
[c] Department of Pediatric Neurology, Baylor College of Medicine, Houston, USA
[d] Division of Neurology, Clinical Research Institute, Kanagawa Children's Medical Center, Yokohama, Japan

ARTICLE INFO

Article history:
Received 24 February 2012
Accepted 24 February 2012
Available online xxxx

Keywords:
Treatment
Protein misfolding
Hypomyelinating disease
CNS
Food compound
Model mouse

ABSTRACT

PLP1 amino acid substitutions cause accumulation of misfolded protein and induce endoplasmic reticulum (ER) stress, causing Pelizaeus–Merzbacher disease (PMD), a hypomyelinating disorder of the central nerve system. Currently no effective therapy is available for PMD. Promoted by its curative effects in other genetic disease models caused by similar molecular mechanisms, we tested if curcumin, a dietary compound, can rescue the lethal phenotype of a PMD mouse model (*myelin synthesis deficient, msd*). Curcumin was administered orally to *myelin synthesis deficit* (*msd*) mice at 180 $mg \cdot kg^{-1} \cdot day^{-1}$ from the postnatal day 3. We evaluated general and motor status, changes in myelination and apoptosis of oligodendrocytes by neuropathological and biochemical examination, and transcription levels for ER-related molecules. We also examined the pharmacological effect of curcumin in cell culture system. Oral curcumin treatment resulted in 25% longer survival ($p<0.01$). In addition, oligodendrocytes undergoing apoptosis were reduced in number ($p<0.05$). However, no apparent improvement in motor function, neurological phenotype, and myelin formation was observed. Curcumin treatment did not change the expression of ER stress markers and subcellular localization of the mutant protein *in vitro* and/or *in vivo*. Curcumin partially mitigated the clinical and pathological phenotype of *msd* mice, although molecular mechanisms underlying this curative effect are yet undetermined. Nonetheless, curcumin may serve as a potential therapeutic compound for PMD caused by *PLP1* point mutations.

1. Introduction

Pelizaeus–Merzbacher disease (PMD) is a devastating X-linked neurodevelopmental disease characterized by a failure of myelination in the central nervous system (CNS) [1,2]. Clinical symptoms of PMD include nystagmus, spastic quadriplegia, ataxia, dystonia, and developmental delay. Mutations in the proteolipid protein gene (*PLP1*), encoding a major myelin membrane protein, are responsible for PMD [3]. *PLP1* mutations include genomic duplication, deletion, and point mutations, each of which leads to CNS dysmyelination through distinct molecular mechanisms [1,2]. Despite all that is known about PMD, no effective therapy has been established to date. *PLP1* point mutations, many of which lead to amino acid substitutions, cause improper folding and accumulation of the mutant proteins in the endoplasmic reticulum (ER), resulting in disruption of ER homeostasis and induction of apoptosis of oligodendrocytes mediated by unfolded protein response (UPR) [4,5]. Thus, modulation of this pathological process may mitigate the manifestation of PMD.

Recently, curcumin (diferuloylmethane), a polyphenol dietary compound derived from the curry spice turmeric, has been used in several therapeutic strategies to rescue rodent models from genetic diseases caused by mutations that lead to protein misfolding. Four genes responsible for 3 major genetic disorders, *CFTR* (cystic fibrosis; CF), *MPZ* and *PMP22* (Charcot-Marie-Tooth disease type 1; CMT1), and *RHO* (retinitis pigmentosa), have been targeted by this treatment both *in vitro* and *in vivo*, and improvements in cellular and clinical phenotypes have been reported [6–9]. These findings implicated that curcumin ameliorates the phenotypes of protein misfolding diseases, including PMD. In this study, we examined the therapeutic effect of oral curcumin administration in a PMD model mouse, *myelin synthesis deficient* (*msd*), carrying a spontaneous A242V missense mutation in the *PLP1* gene.

2. Materials and methods

2.1. Ethical statement

All animals were maintained and utilized in the study according to the institutional guidelines of the National Center for Neurology and

* Corresponding author at: Department of Mental Retardation and Birth Defect Research, National Institute of Neuroscience, National Center of Neurology and Psychiatry, 4-1-1 Ogawahigashi, Kodaira, Tokyo 187-8502, Japan. Fax: +81 423461743.
E-mail address: kinoue@ncnp.go.jp (K. Inoue).

1096-7192/$ – see front matter © 2012 Elsevier Inc. All rights reserved.
doi:10.1016/j.ymgme.2012.02.016

Psychiatry animal care committee and approval of all experimental protocols (2011018).

2.2. Animals, treatment, and phenotypic evaluation

Msd mice [10] were maintained on a B6C3F1/J background. Wild-type male littermates served as controls. In each cage, 6 newborn mice and their mother were housed until the weaning at 1 month after birth, considering the delayed growth of the *msd* mice. Treated and untreated groups were separated by cage. Curcumin (Sigma, C7727) was dissolved in commercially available milk for rodents (10 mg/ml), and was orally administered via a micropipette 6 days/week at 180 mg/kg/day starting at P3. We determined the amount of curcumin according to the previous studies in mice and humans. The same amount of milk was given to the untreated mice. High bioavailability of curcumin in the brain was shown [8]. Essentially, all evaluations were performed in a blinded fashion. The wire hanging test was utilized to evaluate motor performance [11]. Mice were placed on a wire mesh, which was then inverted; latency to fall was recorded. Each mouse was tested 3 times with a 10-min interval between the tests.

2.3. Neuropathological analyses

Mouse brains were fixed with 4% paraformaldehyde in phosphate buffered saline (PBS) and embedded in paraffin using a standard protocol. Coronal serial sections (6 mm thick) around Bregma P1.4 mm were subjected to immunostaining using the following antibodies: mouse anti-myelin basic protein (MBP, SMI99, 1:1000, Covance), rabbit anti-active Caspase3 (#9661, 1:400, Cell Signaling), mouse anti-2′,3′-cyclic nucleotide 3′-phosphodiesterase (CNPase, SMI91, 1:500, Covance), mouse anti-glial fibrillary acidic protein (GFAP, MAB3402 1:1000, Chemicon), and mouse anti-neuronal nuclei (NeuN, A60, 1:1000, Chemicon). For the Terminal deoxynucleotidyl transferase dUTP nick end labeling (TUNEL) assay, we utilized the ApopTag Peroxidase In Situ Apoptosis Detection Kit (Chemicon). For the bright field signal detection, we used biotinylated secondary antibody and peroxidase-conjugated avidin–biotin complex (VECTASTAIN Elite ABC kit, Vector Laboratories) with either ImmPACT DAB or NovaRED (Vector Laboratories). For the fluorescent double staining, Alexa fluor-conjugated secondary antibodies (Molecular Probes) were used followed by visualization using the FLUOVIEW Laser scanning microscope (Olympus).

2.4. Quantification of MBP by enzyme-linked immunosorbent assay (ELISA)

Brains were obtained from treated or untreated *msd* and wild-type mice at P21 (3 animals for each group). A 2-mm-thick coronal slice around Bregma P1.4 mm was sonicated in lysis buffer (20 mM Tris–HCl, pH 6.8, 1% SDS, 4 mM EDTA), followed by centrifugation at 12,000 rpm for 30 min to obtain supernatants. Standard sandwich ELISA was utilized for the MBP measurement using mouse anti-MBP antibody (1:1000, Covance) for coating the microtiter plates and rabbit anti-MBP antibody (1:1000, Dako) for detection using SureBlue Reserve TMB Microwell Peroxidase substrate (KPL). Protein concentrations were determined by measurements at 450 nm using a plate reader (1420 Multilabel Counter, Perkin Elmer). The measurement was repeated 4 times for each animal.

2.5. Electron microscopic analysis of the optic nerve

Optic nerves were isolated and fixed in 2% glutaraldehyde and 2% paraformaldehyde in 0.1 M PBS (pH 7.4), followed by postfixation in 1% osmium (OsO4) in PBS. After serial dehydration, the optic nerves were flat-embedded in Epon. Serial ultrathin sections cut at 70 nm were examined under an electron microscope (model H-600, Hitachi). Semi-thin sections cut at 1 mm were stained with toluidine blue and examined under a bright field microscope for quantification of myelinated fibers.

2.6. Quantitative reverse transcriptase (RT)-PCR

We isolated internal capsule (IC) from sliced fresh brains (3 animals for each group) by punching the IC out using a chopped micropipette tip. Total RNA was extracted from the IC and spinal cords using RNeasy Protect Mini Kit (Qiagen) and was converted to cDNA using Superscript III reverse transcriptase and random primers (Invitrogen). We determined the transcript levels for the genes listed below using pre-designed TaqMan probes (Applied Biosystems) and synthesized cDNA as templates for quantitative RT-PCR (7900HT, Applied Biosystems). The assay IDs for the specific genes were: *Grp78/Bip*: Mm00517691, *Herpud1*: Mm00445600, *calnexin*: Mm00500330, *calreticulin*: Mm00482936, *Chop*: Mm00492097, *Gadd45a*: Mm00432802, *Actb*: Mm00607939. Relative measurement to *Actb* was calculated using the DDCT method following the manufacturer's standard protocol.

2.7. Cell culture and in vitro expression studies

Human *PLP1* cDNA, either wild-type or A242V mutant, was cloned into a strong mammalian expression vector, pCAG, under cytomegalovirus and actin promoters and fused with the FLAG tag to the carboxyl terminus of PLP1 to generate pCAG-PLP1wt-FLAG and pCAG-PLP1msd-FLAG. HeLa cells (originally obtained from ATCC; cat#CCL-2), maintained in DMEM with 10% FBS, were transfected with 2 mg of plasmid DNA using TransIt LT1 (Miruas). Twenty-four hours later, cells were treated with curcumin (10 mg/ml in DMSO) or vehicle (DMSO) for 6 h at various concentrations and harvested for the extraction of total RNA, which was then converted to cDNA. We determined the expression level of the same 6 genes associated with unfolded protein response (UPR) along with *GAPDH* as a control, using human pre-designed TaqMan probes (Applied Biosystems).

HeLa cells treated with curcumin for 12 h were transfected with pCAG-PLP1msd-FLAG. After 24 h of incubation, cell surface proteins were biotinylated as described elsewhere [12]. Cells were harvested with streptavidin beads (Pierce) to isolate the plasma membrane fraction. Similarly, cells were treated with 0.01% digitonin to obtain the plasma membrane and cytosolic fractions. After the collection of the supernatant, cells were harvested with 1% Triton and 0.1% SDS to obtain the organelle and nuclear fractions. Protein extracts from each fraction were used for western blotting with mouse anti-FLAG antibody (Sigma, M2, 0.5 mg/ml).

HeLa cells transfected with pCAG-PLP1wt-FLAG and pCAG-PLP1msd-FLAG were fixed with 4% paraformaldehyde and subjected to fluorescent immunocytochemistry with double labeling using the mouse anti-FLAG and rabbit anti-calnexin (Enzo, ADI-SPA-860, 1:200) antibodies, followed by visualization with a confocal laser microscope (FV-1000, Olympus).

2.8. Statistical analyses

For survival analysis (Fig. 1A), we used Kaplan–Meier method combined with a generalized Wilcoxon test. For the motor function analysis (Fig. 1C), we used one-way analysis of variance (ANOVA) and Student's *t*-test. For the ELISA (Fig. 2B), we used a repeated measures analysis of variance using the residual maximum likelihood (REML). For the quantification of myelin fibers (Fig. 2D), we used one-way ANOVA and Student's *t*-test. For the TUNEL and caspase3 assays (Figs. 3 and 4), we used a repeated measures analysis of variance using the REML. For the quantitative RT-PCR analyses (Fig. 5 and Fig S1), we used one-way ANOVA and Student's *t*-test. Mainly, means ± standard deviations were shown in the figures. All statistical examination was carried out using JMP software (SAS Institute).

Please cite this article as: L.-H. Yu, et al., Effect of curcumin in a mouse model of Pelizaeus–Merzbacher disease, Mol. Genet. Metab. (2012), doi:10.1016/j.ymgme.2012.02.016

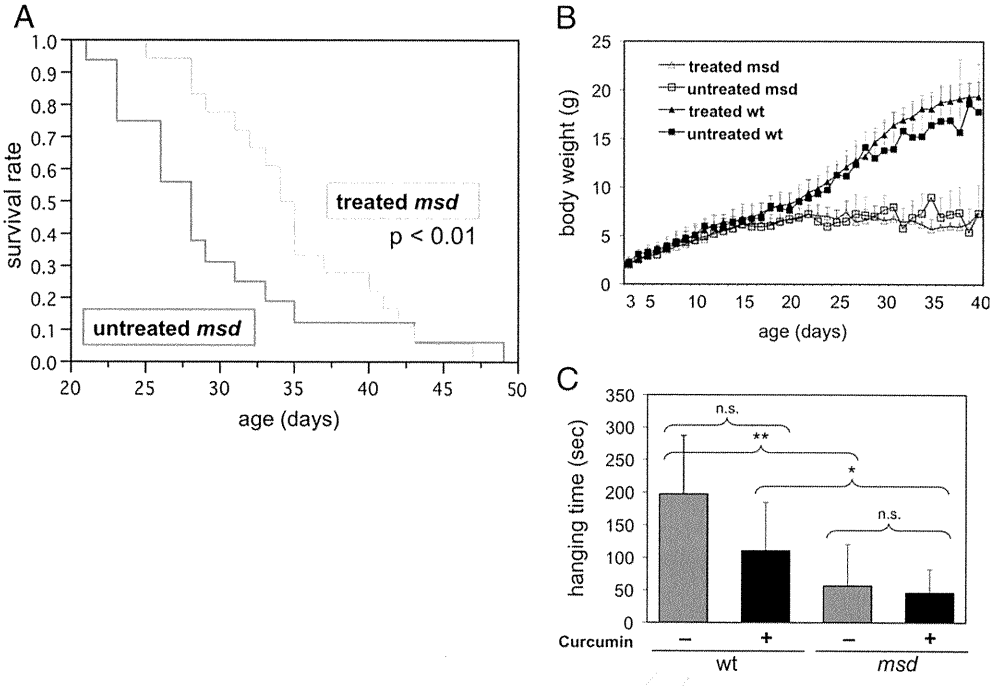

Fig. 1. Effect of curcumin on the lifespan, growth curve and motor performance of *msd* mice. A. Survival curves of treated *msd* mice (n = 18, green) and untreated mice (n = 16, red). The life spans of treated mice were statistically longer than those of untreated mice. Data from wild-type mice were not shown because no mouse died during the course of the study regardless of treatment. B. Body weight changes are shown for treated *msd* (open triangle, n = 41), untreated *msd* (open square, n = 17), treated wild-type (closed triangle, n = 35) and untreated wild-type (open square, n = 17) mice. *Msd* mice showed growth retardation from 3 weeks of age; curcumin treatment had no effect on this growth retardation. The data are presented as mean ± SD. C. Motor function was evaluated by the wire hanging test. The data are presented as mean ± SD. Untreated wild-type (left gray bar: n = 5); treated wild-type (left filled bar: n = 4); untreated *msd* (right gray bar: n = 10); and treated *msd* (right filled bar: n = 11). Statistical significances are shown as asterisks: * $p<0.05$; ** $p<0.01$. n.s. = not significant. *Msd* mice fell significantly earlier than wild-type mice regardless of treatment. No significant difference was observed between treated and untreated *msd* mice.

3. Results

3.1. Curcumin extended the lifespan of msd mice

All experiments were performed in 4 groups of male mice: treated or untreated *msd* mice, and treated or untreated wild-type mice. In general, neurological symptoms of *msd* mice initiated at postnatal day 7 (P7) with moderate tremors, which gradually worsened, followed by dystonia occurring around P21. All *msd* mice died within 2 months due to prolonged severe dystonic cramps, which resulted in respiratory failure. When treated with curcumin, *msd* mice lived for a median of 35 days (ranging from 25 to 47 days, Fig. 1A), which

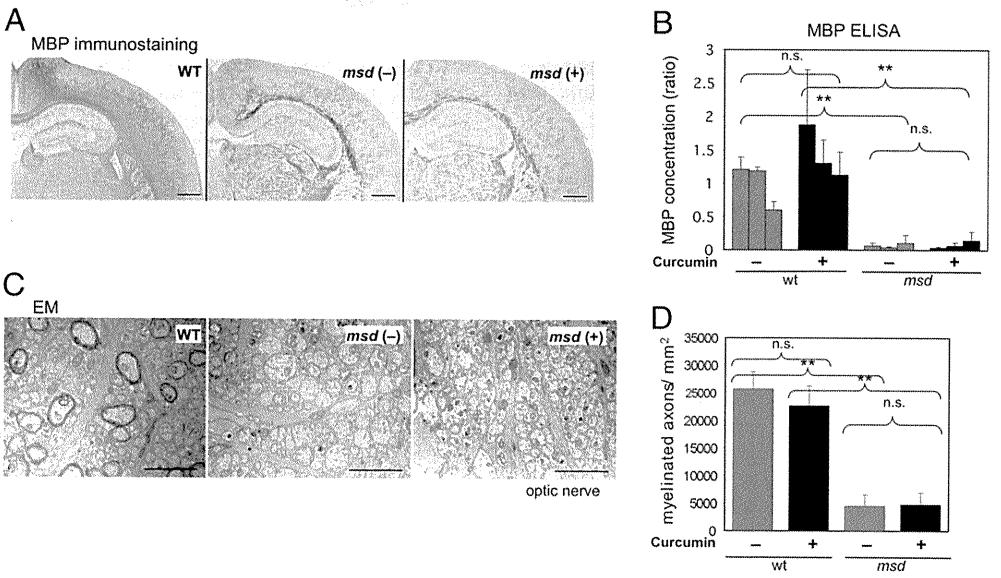

Fig. 2. Curcumin did not ameliorate CNS dysmyelination. A. Coronal sections of P21 mouse brains with MBP immunostaining are shown. Both treated and untreated *msd* brains (*msd* (−) and *msd* (+), respectively) showed sparse and weak staining in the white matter and cortex in comparison with the untreated wild-type brains (WT). All slides were stained simultaneously to avoid variation in staining due to the difference in wash and incubation times. Scale bars show 500 mm. B. Quantification of MBP in isolated IC by ELISA at P21 (n = 3). Relative amounts to the average of untreated wild-type mice are shown. Note that *msd* mice, regardless of treatment, showed extremely low amounts of MBP and the treatment did not change the protein expression level. The data are presented as mean ± SD. C. Coronal sections of optic nerves examined by electron microscopy at P14 are shown in the same order as A. In comparison with untreated wild-type mice, both treated and untreated *msd* mice optic nerves barely exhibited myelinated axons. Scale bar shows 2 mm. No apparent improvement by curcumin treatment was observed at P21 and P28 (data not shown). D. Number of myelin fibers in optic nerves was counted using the same specimen as C stained with toluidine blue (n = 3 in each group). Treated and untreated *msd* mice showed no significant difference in the number of myelinated fibers, which were significantly fewer than in wild-type mice. The data are presented as mean ± SD. Statistical significances are shown as asterisks: * $p<0.05$; ** $p<0.01$; n.s. = not significant.

Please cite this article as: L.-H. Yu, et al., Effect of curcumin in a mouse model of Pelizaeus–Merzbacher disease, Mol. Genet. Metab. (2012), doi:10.1016/j.ymgme.2012.02.016

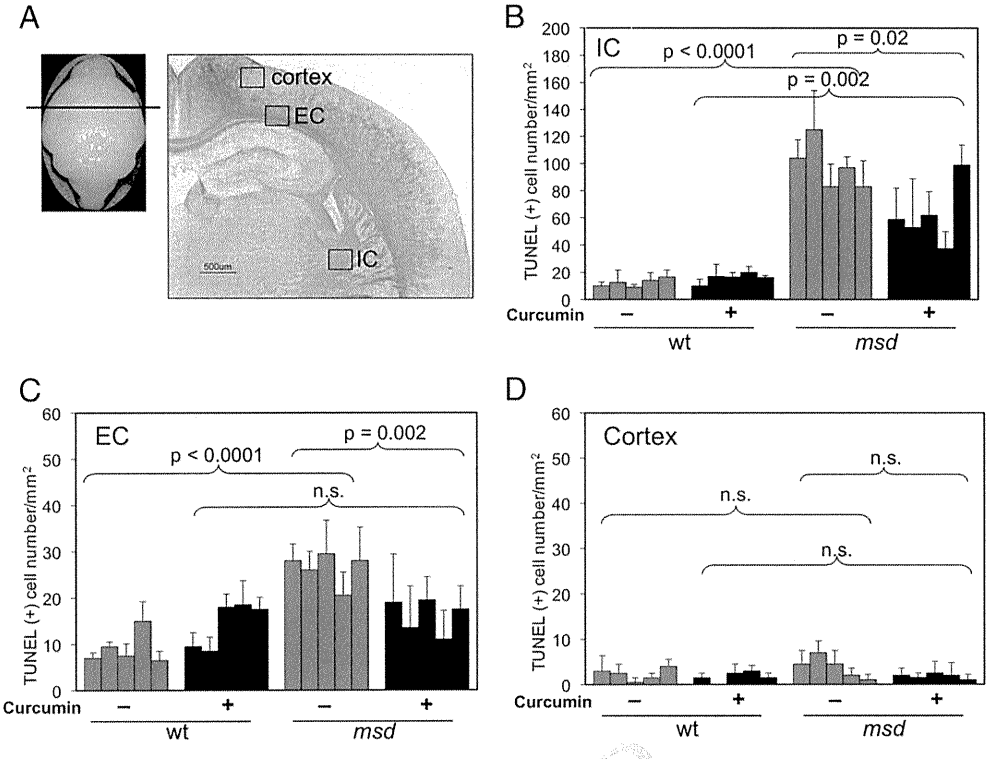

Fig. 3. Quantification of TUNEL-positive apoptotic cells. A. P21 mouse brain showing the position of examination (left; horizontal bar). Coronal section of P21 wild-type mouse brain shows the areas of examination (right; boxes). B–D. TUNEL-positive cells were microscopically counted in the white matter (internal capsule, IC; external capsule; EC) and the parietal cortex (M1 and M2 area) at P21 under a bright field microscope at 100-fold magnification. Each bar represents an averaged TUNEL-positive cell number per mm^2 (4 fields examined) in each mouse. The data were presented as mean ± SD. Both in the IC (B) and EC (C), untreated *msd* mice showed enhanced apoptosis. Treated *msd* mice showed significantly fewer number of TUNEL-positive cells than untreated *msd* mice. In the EC of the treated *msd*, apoptotic cell number was reduced to the level of wild-type mice. Untreated wild-type (gray bars: n = 5); treated wild-type (blue bars: n = 5); untreated *msd* (red bars: n = 5); treated *msd* (green bars: n = 5) mice. n.s. = not significant.

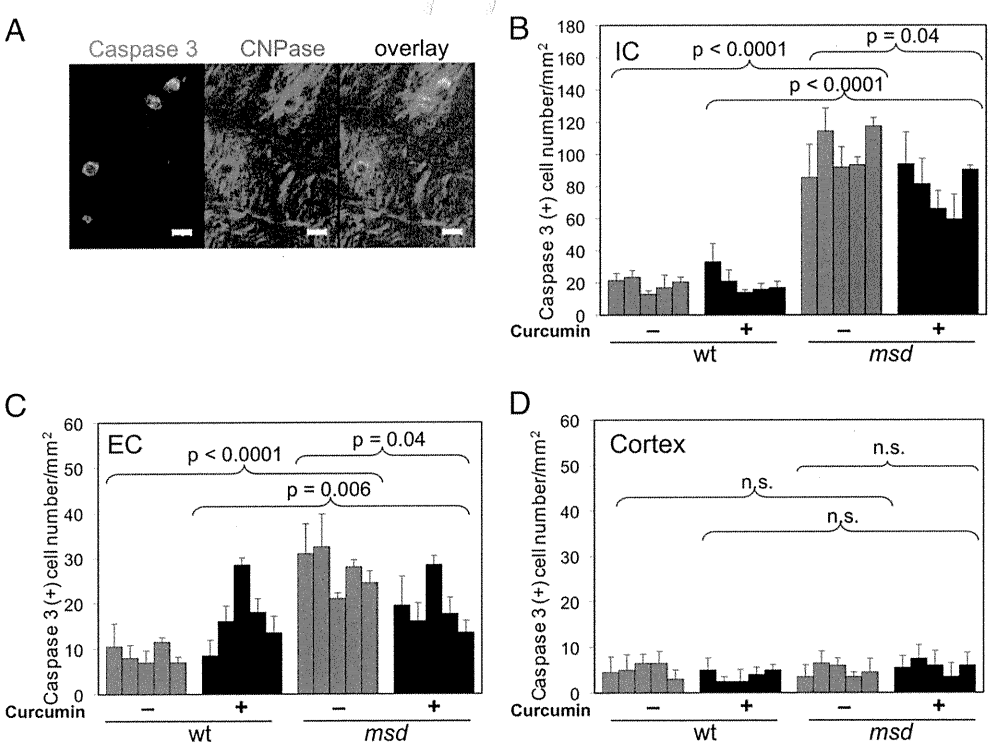

Fig. 4. Quantification of active caspase3-positive apoptotic cells by immunohistochemistry. A. Fluorescent double staining of active caspase3 (left; green) and CNPase (middle; red) visualized by confocal microscopy demonstrated cytoplasmic overlapping signals (right; overlay) (scale bar shows 100 mm). Note that detection of cytoplasmic staining of CNPase required an overexposure of myelin sheath staining. B–D. Active caspase3-positive cells were quantified in the white matter (IC and EC) and the parietal cortex in P21 mice. The experimental design was same as the TUNEL assay demonstrated in Fig. 2. In the IC and EC (but not the cortex), untreated *msd* mice showed enhanced apoptosis. Treated *msd* mice showed significantly fewer numbers of caspase3-positive cells than untreated *msd* mice. The data are presented as mean ± SD. n.s. = not significant.

Please cite this article as: L.-H. Yu, et al., Effect of curcumin in a mouse model of Pelizaeus–Merzbacher disease, Mol. Genet. Metab. (2012), doi:10.1016/j.ymgme.2012.02.016

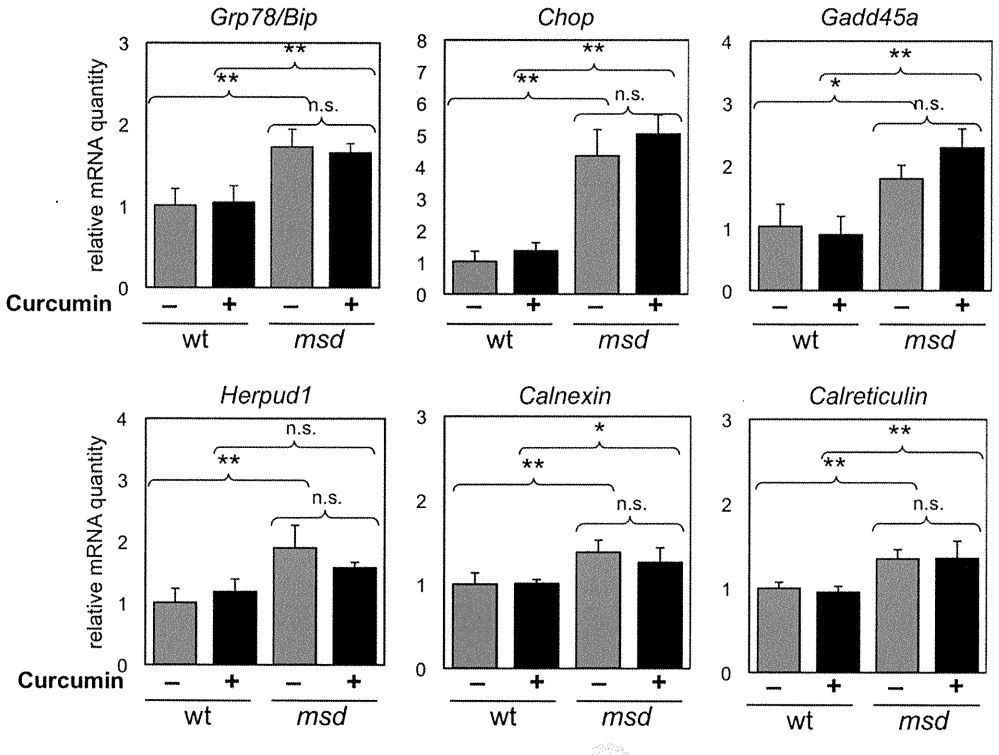

Fig. 5. Quantitative RT-PCR analyses for genes associated with UPR in *msd* mice expression levels for *Grp78/Bip*, *Chop*, *Gadd45a*, *Herpud1*, *calnexin*, and *calreticulin* were determined in the isolated IC at P14. *Gapdh* was used as an inner control. Each column represents untreated wild-type (n = 3, gray bar), treated wild-type (n = 3, blue bar), untreated *msd* (n = 3, red bar), and treated *msd* (n = 3, green bar) mice. Ratios to untreated wild-type mice are shown. The data are presented as mean ± SD. Statistical significances are shown as asterisks: * $p<0.05$; ** $p<0.01$; n.s. = not significant.

was 7 days longer than the untreated *msd* mice (median of 28 days ranging from 21 to 49 days, $p<0.01$). Curcumin had no effect on the survival of wild-type mice.

Besides the ~25% longer survival, difference in neurological phenotypes between treated and untreated mice, including onset and severity of tremor, gait disturbance, and frequency and severity of dystonic cramping, was not obvious by observation. Additionally, no difference was noted in the growth curve and motor function as determined by the wire hanging test between treated and untreated *msd* mice (Figs. 1B and C).

3.2. Curcumin did not ameliorate CNS dysmyelination

Given the effects of curcumin on survival of *msd* mice, we then determined if this beneficial effect of curcumin could further ameliorate dysmyelination in the CNS. First, we examined the expression of myelin basic protein (MBP), a major component of the mature myelin sheath, to evaluate myelin formation by immunohistochemistry (Fig. 2A). Based on the MBP expression profile determined in wild-type mice, we decided to evaluate myelin formation at P21. In the white matter (IC and external capsule (EC), respectively) of the untreated *msd* brains, MBP-positive myelin fibers were present sparsely and weakly when compared to wild-type mice. Treated *Msd* mice also showed similarly sparse MBP-positive myelin fibers, which was essentially indistinguishable from untreated mice.

Next, we measured the MBP protein level using ELISA (Fig. 2B). In wild-type mice, MBP protein increased more than twice from P14 to P21, representing a progression of myelination (P14 data not shown). Untreated *msd* mice showed only ~5 to 10% amount of wild-type mice at P21, consistent with the findings in immunohistochemistry. We observed no significant increase in the amount of MBP for treated *msd* mice both at P14 and P21, also confirming the immunohistochemistry findings.

In addition, we examined the ultrastructure of the myelin sheath by electron microscopic analysis of optic nerves at P21 (Fig. 2C). While myelin ensheathement was apparent around large axons in wild-type mice, almost no myelin was observed in untreated *msd* mice. Similarly, treated *msd* mice showed only unmyelinated axons. We also quantified the number of myelinated axons in toluidine blue-stained sections and found that treated and untreated *msd* mice both showed similarly reduced number of myelinated fibers (Fig. 2D). Altogether, curcumin did not ameliorate dysmyelination in *msd* mice and the extended lifespan was unlikely to be the result of improvement in myelination.

3.3. Curcumin mitigated apoptosis of oligodendrocytes

Next, we examined the effect of curcumin on the apoptotic cell death of oligodendrocytes at P21. In *msd* mice, TUNEL- and caspase 3-positive apoptotic cells were increased in the white matter (IC and EC) where oligodendrocytes predominate the cell population, but were not in the cortex (Figs. 3 and 4). A double-labeling study showed that the vast majority of either TUNEL- or caspase3-positive cells were also positive for CNPase, but were barely positive for GFAP or NeuN (Fig. 4A, Table 1). These findings suggest that cells undergoing apoptosis in the white matter of the *msd* brains are predominantly oligodendrocytes [4].

Upon curcumin administration, the treated *msd* mice showed significant decreases in the number of TUNEL-positive apoptotic cells in the white matter compared to the untreated mice (Fig. 3). No such change was observed in the wild-type mice. We also observed similar findings in active caspase3-positive cells both in the IC and EC (Figs. 4B–D). These results suggest that curcumin can mitigate the apoptotic cell death of oligodendrocytes in the *msd* mouse brain.

3.4. Effects of curcumin on the expression of UPR markers and the subcellular localization of mutant PLP1 protein

Next, we determined if curcumin could change the expression of genes associated with UPR, as observed in retinitis pigmentosa study

Please cite this article as: L.-H. Yu, et al., Effect of curcumin in a mouse model of Pelizaeus–Merzbacher disease, Mol. Genet. Metab. (2012), doi:10.1016/j.ymgme.2012.02.016

Table 1
Double labeling studies with cell-specific markers and TUNEL or active caspase3.

Cell-specific markers	Number of double (+) cells/ TUNEL(+) cells (%)			Number of double (+) cells/ caspase3(+) cells (%)		
	Cortex	IC[c]	EC[d]	Cortex	IC[a]	EC[b]
CNPase	7/ 7(100)	226/ 226(100)	49/ 49(100)	7/ 7(100)	79/ 79(100)	22/ 22(100)
GFAP	0/10(0)	10/255(4.0)	0/57(0)	0/5(0)	0/68(0)	0/21(0)
NeuN	0/17(0)	9/207(4.3)	1/58(1.7)	1/ 6(16.7)	3/71(4.2)	0/22(0)

Number of cells double-positive for the apoptotic marker (either TUNEL or active caspase3) and the cell specific marker (CNPase, GFAP, or NeuN) per number of all cells positive for the apoptotic marker were shown. For example, in the TUNEL assay (left), 49 cells were found to be TUNEL-positive in EC and all of these 49 cells were also positive for CNPase (this does not mean that all CNPase-positive cells were also positive for TUNEL). Cells were counted in a total of 4 fields (100-fold magnification). Proportion of the cells positive for both TUNEL and cell-specific marker are shown in the parenthesis. Note that a large number of cells positive for TUNEL or caspase3 predominated in IC and EC. Most of them were double positive for CNPase and few were positive for GFAP or NeuN.
a: IC; internal capsule. b: EC; external capsule.

[9]. We examined 6 genes, namely *Grp78/Bip*, *Chop*, *Herpud1*, *Gadd45a*, *calnexin*, and *calreticulin* [13], in the IC by quantitative RT-PCR. We observed significant upregulation of all genes in *msd* mice with *Chop* showing the largest increase at P14 (Fig. 5), as previously reported [14,15]. However, curcumin treatment did not attenuate the expression of these genes.

Because a large number of oligodendrocytes undergoing apoptosis would be removed promptly from the *msd* brain, potentially concealing the attenuation effect of curcumin from detection *in vivo*, we also examined the same genes in a culture system using HeLa cells that transiently expressed mutant PLP1 to determine the direct effect of curcumin. Again, mutant PLP1 upregulated the expression of at least 4 out of 6 UPR genes (Fig S1A). However, curcumin treatment did not attenuate the expression of UPR genes (Fig S1B). These *in vivo* and *in vitro* findings suggest that the effect of curcumin may not be associated with UPR gene expression, at least in our experimental setting.

Next, we examined if curcumin changed the subcellular localization of accumulated mutant PLP1 proteins from the ER to the cytoplasm or plasma membrane, as observed in the CF and CMT1 studies [6–8]. HeLa cells were transiently transfected with a mutant *PLP1* plasmid and then examined by subcellular fractionation and western blotting (Figs. S2A and B). Mutant PLP1 showed only a faint signal in both fractions, which was not enhanced by curcumin treatment. In an immuno-cytochemistry study co-stained with an ER marker, calnexin, curcumin did not promote apparent translocation of the mutant PLP1 protein, while wild-type PLP1 appeared to show enhanced staining on cytoplasmic membrane after curcumin treatment (Fig. S2C).

4. Discussion

As therapeutic reagents for rare genetic disorders (especially in children), food compounds have considerable advantages with respect to safety, ethical issues, and material availability, as well as potential in clinical applications. In this study, we demonstrated that curcumin could serve as a potential therapeutic compound for PMD. Oral curcumin treatment extended the lifespan of *msd* mice by ~25% as compared to untreated mice. Although this extended survival was not accompanied by reconstitution of the CNS myelin and recovery in motor function, it inhibited apoptotic cell death in oligodendrocytes. As far as we know, curcumin represents the first compound that can mitigate the lethal phenotype caused by *PLP1* point mutations in the mouse. Because curcumin is a dietary compound with proven clinical safety in humans, it can be readily applied to patients with PMD that is caused by *PLP1* point mutations.

The exact mechanisms for the therapeutic action of curcumin were not fully elucidated. Curcumin has been reported to reduce oxidative damage, prevent amyloid formation, and decrease inflammation in the treatment of various neurodegenerative diseases and cancers by altering the activity of NF-kB, AKT/mTOR, AP-1, NFR2, and protein kinases [16]. In addition, curcumin acts as an inhibitor of the sarco/endoplasmic reticulum Ca^{2+} ATPase (SERCA), presumably modifying ER stress [17]. Because the pathological processes of PMD involve not only protein misfolding and ER stress but also chronic inflammation [18,19], curcumin may elicit multifaceted pharmacological actions that work together to reduce oligodendrocyte cell death.

The modest therapeutic effects observed in *msd* mice contrasted with the dramatic improvement in the peripheral myelin in heterozygous *Tr-J* mice [8]. It is possible that curcumin may have limited therapeutic effects on genetically severe alleles. Massive apoptotic cell death of oligodendrocytes occurring at early postnatal stage would eliminate a major population of oligodendrocytes in *msd*. This would be more difficult to overcome than diseases with slower progression, like CF or CMT1. In fact, curcumin was not curative on the homozygous *Tr-J* allele, which causes a severe peripheral hypomyelination and death within a month (personal communication, M. Khajavi, JR Lupski). It is also possible that *msd* mutant PLP1 protein has stronger property to be stuck in ER than CFTR Δ508 or PMP22 *Tr-J*, which are relatively milder disease alleles. In fact, curcumin may promote membrane trafficking of wild-type PLP1 (Fig. 7). Possibly, curcumin treatment on milder *PLP1* alleles may confer more obvious curative effects.

In conclusion, we demonstrated that a dietary compound, curcumin, is a potential therapeutic compound for patients with PMD carrying *PLP1* point mutations. As far as we know, this is the first study demonstrating such therapeutic effect on PMD *in vivo*. Because of its safety and wide applicability in humans, as evidenced in over 60 clinical trials [20], further evidence of the ability of curcumin to mitigate the PMD phenotype is awaited.

Acknowledgments

We thank Dr. W. B. Macklin (Cleveland Clinic Foundation, OH) for providing *msd* mice, Drs. I. Miyoshi, N. Yonemoto, and L. Goto (National Center for Neurology and Psychiatry, Japan) for their help in the statistical analyses, Dr. S. Yamashita (Kanagawa Children's Medical Center) for his advice in electron microscopic analysis and Harumi Iwashita and Eriko Arima for their technical assistance and animal care. This study was supported in part by grants from the Heath and Labour Sciences Research Grants, Research on Intractable Diseases (KI, H22-Nanchi-Ippan-132), Grants-in-Aid for Scientific Research from the Ministry of Education, Culture, Sports, Science and Technology, Japan (KI, 21390103 and 23659531), and a Grant from Takeda Science Foundation (KI).

Appendix A. Supplementary data

Supplementary data to this article can be found online at doi:10.1016/j.ymgme.2012.02.016.

References

[1] K. Inoue, PLP1-related inherited dysmyelinating disorders: Pelizaeus–Merzbacher disease and spastic paraplegia type 2, Neurogenetics 6 (2005) 1–16.
[2] J.Y. Garbern, Pelizaeus–Merzbacher disease: genetic and cellular pathogenesis, Cell Mol. Life Sci. 64 (2007) 50–65.
[3] J. Garbern, F. Cambi, M. Shy, J. Kamholz, The molecular pathogenesis of Pelizaeus–Merzbacher disease, Arch. Neurol. 56 (1999) 1210–1214.
[4] A. Gow, C.M. Southwood, R.A. Lazzarini, Disrupted proteolipid protein trafficking results in oligodendrocyte apoptosis in an animal model of Pelizaeus–Merzbacher disease, J. Cell Biol. 140 (1998) 925–934.
[5] C.M. Southwood, J. Garbern, W. Jiang, A. Gow, The unfolded protein response modulates disease severity in Pelizaeus–Merzbacher disease, Neuron 36 (2002) 585–596.

Please cite this article as: L.-H. Yu, et al., Effect of curcumin in a mouse model of Pelizaeus–Merzbacher disease, Mol. Genet. Metab. (2012), doi:10.1016/j.ymgme.2012.02.016

[6] M.E. Egan, M. Pearson, S.A. Weiner, V. Rajendran, D. Rubin, J. Glockner-Pagel, S. Canny, K. Du, G.L. Lukacs, M.J. Caplan, Curcumin, a major constituent of turmeric, corrects cystic fibrosis defects, Science 304 (2004) 600–602.
[7] M. Khajavi, K. Inoue, W. Wiszniewski, T. Ohyama, G.J. Snipes, J.R. Lupski, Curcumin treatment abrogates endoplasmic reticulum retention and aggregation-induced apoptosis associated with neuropathy-causing myelin protein zero-truncating mutants, Am. J. Hum. Genet. 77 (2005) 841–850.
[8] M. Khajavi, K. Shiga, W. Wiszniewski, F. He, C.A. Shaw, J. Yan, T.G. Wensel, G.J. Snipes, J.R. Lupski, Oral curcumin mitigates the clinical and neuropathologic phenotype of the Trembler-J mouse: a potential therapy for inherited neuropathy, Am. J. Hum. Genet. 81 (2007) 438–453.
[9] V. Vasireddy, V.R. Chavali, V.T. Joseph, R. Kadam, J.H. Lin, J.A. Jamison, U.B. Kompella, G.B. Reddy, R. Ayyagari, Rescue of photoreceptor degeneration by curcumin in transgenic rats with P23H rhodopsin mutation, PLoS One 6 (2011) e21193.
[10] S. Gencic, L.D. Hudson, Conservative amino acid substitution in the myelin proteolipid protein of jimpy^{msd} mice, J. Neurosci. 10 (1990) 117–124.
[11] K. Kitamura, Y. Itou, M. Yanazawa, M. Ohsawa, R. Suzuki-Migishima, Y. Umeki, H. Hohjoh, Y. Yanagawa, T. Shinba, M. Itoh, K. Nakamura, Y. Goto, Three human ARX mutations cause the lissencephaly-like and mental retardation with epilepsy-like pleiotropic phenotypes in mice, Hum. Mol. Genet. 18 (2009) 3708–3724.
[12] T. Morimura, M. Hattori, M. Ogawa, K. Mikoshiba, Disabled1 regulates the intracellular trafficking of reelin receptors, J. Biol. Chem. 280 (2005) 16901–16908.
[13] I. Kim, W. Xu, J.C. Reed, Cell death and endoplasmic reticulum stress: disease relevance and therapeutic opportunities, Nat. Rev. Drug Discov. 7 (2008) 1013–1030.
[14] L.D. Hudson, N.L. Nadon, Amino acid substitutions in proteolipid protein that cause dysmyelination, in: R.E. Martenson (Ed.), Myelin: biology and chemistry, CRC press, Boca Raton, 1992, pp. 677–702.
[15] C. Southwood, A. Gow, Molecular pathways of oligodendrocyte apoptosis revealed by mutations in the proteolipid protein gene, Microsc. Res. Tech. 52 (2001) 700–708.
[16] J.S. Jurenka, Anti-inflammatory properties of curcumin, a major constituent of Curcuma longa: a review of preclinical and clinical research, Altern. Med. Rev. 14 (2009) 141–153.
[17] J.G. Bilmen, S.Z. Khan, M.H. Javed, F. Michelangeli, Inhibition of the SERCA Ca^{2+} pumps by curcumin. Curcumin putatively stabilizes the interaction between the nucleotide-binding and phosphorylation domains in the absence of ATP, Eur. J. Biochem. 268 (2001) 6318–6327.
[18] J.M. Edgar, M.C. McCulloch, P. Montague, A.M. Brown, S. Thilemann, L. Pratola, F.I. Gruenenfelder, I.R. Griffiths, K.A. Nave, Demyelination and axonal preservation in a transgenic mouse model of Pelizaeus–Merzbacher disease, EMBO Mol. Med. 2 (2010) 42–50.
[19] C.L. Tatar, S. Appikatla, D.A. Bessert, A.S. Paintlia, I. Singh, R.P. Skoff, Increased *Plp1* gene expression leads to massive microglial cell activation and inflammation throughout the brain, ASN Neuro 2 (2010) art:e00043.
[20] Curcumin Clinical Trials, http://clinicaltrials.gov/ct2/results?term=curcumin [accessed January 11,2012].

Please cite this article as: L.-H. Yu, et al., Effect of curcumin in a mouse model of Pelizaeus–Merzbacher disease, Mol. Genet. Metab. (2012), doi:10.1016/j.ymgme.2012.02.016